Article

Characterization and Effect of Ag(0) vs. Ag(I) Species and Their Localized Plasmon Resonance on Photochemically Inactive TiO$_2$

Chanel Tri Handoko [1,2], **Nikolaos G. Moustakas [2]**, **Tim Peppel [2,***], **Armin Springer [3]**, **Freddy E. Oropeza [4]**, **Adri Huda [1]**, **Muhammad Djoni Bustan [5]**, **Bambang Yudono [1]**, **Fakhili Gulo [1,***] and **Jennifer Strunk [2]**

[1] Program Studi Ilmu Lingkungan, Universitas Sriwijaya, Jalan Padang Selasa No. 524, Palembang 30121, Sumatera Selatan, Indonesia; chanel@student.pps.unsri.ac.id (C.T.H.); adrihuda@student.pps.unsri.ac.id (A.H.); yudonob@hotmail.com (B.Y.)

[2] Leibniz-Institut für Katalyse e. V. (LIKAT), Albert-Einstein-Str. 29a, 18059 Rostock, Germany; nikolaos.moustakas@catalysis.de (N.G.M.); jennifer.strunk@catalysis.de (J.S.)

[3] Arbeitsbereich Medizinische Biologie und Elektronenmikroskopisches Zentrum (EMZ), Universitätsmedizin Rostock, Strempelstr. 14, 18057 Rostock, Germany; armin.springer@med.uni-rostock.de

[4] Laboratory of Inorganic Materials Chemistry, Department of Chemical Engineering and Chemistry, Eindhoven University of Technology, P.O. Box 513, 5600 MB Eindhoven, The Netherlands; F.E.Oropeza.Palacio@tue.nl

[5] Program Studi Teknik Kimia, Fakultas Teknik, Universitas Sriwijaya, Jalan Palembang-Inderalaya Km. 32, Inderalaya 30862, Sumatera Selatan, Indonesia; djajashanta@yahoo.co.id

* Correspondence: tim.peppel@catalysis.de (T.P.); fgulo@unsri.ac.id (F.G.)

check for updates

Abstract: Commercial TiO$_2$ (anatase) was successfully modified with Ag nanoparticles at different nominal loadings (1%–4%) using a liquid impregnation method. The prepared materials retained the anatase structure and contained a mixture of Ag^0 and Ag^I species. Samples exhibited extended light absorption to the visible region. The effect of Ag loading on TiO$_2$ is studied for the photocatalytic reduction of CO$_2$ to CH$_4$ in a gas–solid process under high-purity conditions. It is remarkable that the reference TiO$_2$ used in this work is entirely inactive in this reaction, but it allows for studying the effect of Ag on the photocatalytic process in more detail. Only in the case of 2% Ag/TiO$_2$ was the formation of CH$_4$ from CO$_2$ observed. Using different light sources, an influence of the localized surface plasmon resonance (LSPR) effect of Ag is verified. A sample in which all Ag has been reduced to the metallic state was less active than the respective sample containing both Ag^0 and Ag$^+$, indicating that a mixed oxidation state is beneficial for photocatalytic performance. These results contribute to a better understanding of the effect of metal modification of TiO$_2$ in photocatalytic CO$_2$ reduction.

Keywords: localized surface plasmon resonance; TiO$_2$; silver; oxidation state; liquid impregnation

1. Introduction

In recent decades, atmospheric CO$_2$ concentration has been increasing annually mainly due to the extensive use of fossil fuels [1,2]. Data from NASA show that in April 2018 the concentration of CO$_2$ reached 407.45 ppm, an increase of 29.23% compared to the respective concentration for April 1958 [2]. As a result, the annual mean global surface temperature increased—as CO$_2$ is a major greenhouse gas contributing to climate change—by 0.99 °C, the highest rise observed since 1880 [3]. Many efforts and experimental research have been focused on the capture of CO$_2$ from the atmosphere and/or its conversion to other economically valuable compounds. Since CO$_2$ is a very stable molecule with a

C = O direct bond energy of +805 kJ/mol, it requires a high energy input for bond cleavage [4]. One of the most promising technologies to convert CO_2 to useful hydrocarbons is the photocatalytic reduction (the chemical transformation of CO_2 through the absorption of photons of appropriate wavelength from a semiconducting material—photocatalyst) which offers a solution for both the energy crisis and global warming [5]. The photocatalytic conversion of CO_2 to value-added hydrocarbons and renewable fuels, such as methane or methanol, is part of a greater effort in the literature to utilize small molecules such as H_2 and CO_2, collectively termed as "artificial photosynthesis" [6–10].

As a semiconductor material, titanium dioxide (TiO_2) has attracted tremendous interest due to its good photocatalytic activity, low toxicity, chemical stability, abundance in nature, and low cost [11,12]. However, there are several factors which hinder the photocatalytic efficiency of TiO_2, such as its absorption range which is limited to wavelengths in the UV region (about 4% of total solar spectrum) [13,14]. Another significant factor reported in many studies is the recombination of charge carriers (electron-hole recombination) in the bulk or the surface of the TiO_2 material [15]. Schneider et al. proposed that nearly 90% of all photogenerated electrons recombine rapidly after the electron excitation process. As a result, this phenomenon triggers low quantum yields (<10%) [16].

Therefore, much effort has been focused on enhancing the photocatalytic activity of TiO_2, including doping with metal or non-metal species [17,18], surface sensitization [19,20], and noble metal deposition [21–25]. In particular, the noble metal deposition has attracted a lot of attention since it can improve e^-–h^+ separation and enhance the semiconductor's absorption in the visible light region [26,27]. Noble metals such as Au, Pt, Ag, Pd, Rh, and coinage metals such as Ni etc., have lower Fermi levels than TiO_2. Therefore, they can act as electron traps, facilitating the separation of charge carriers and preventing their recombination [26]. On the other hand, the localized surface electron plasmon resonance effect (LSPR) induced by noble metals contributes to the activation of TiO_2 absorption in the visible region of the light spectrum.

There are several studies in the literature about photocatalytic CO_2 reduction using Ag/TiO_2 composites [28–32]. The results vary, depending on the materials' synthesis and reaction conditions. For example, previous studies revealed that CH_3OH is the major CO_2 reduction product in liquid-phase experiments, while CH_4 is the main product in gas-phase reactions [33]. A gas-phase system offers several advantages like the variation of the concentration of reactants in a wider range without dissolution phenomena [34]. Furthermore, in gas–solid reactor systems, experiments using high purity conditions can be established as a high vacuum can be applied to eliminate gaseous C-containing impurities from the reaction chamber [35]. Performing CO_2 reduction experiments using conditions of high-purity is extremely important as any source of carbon-containing species can lead to an overestimation of the products. Due to the high stability of the CO_2 molecule, these C-impurities are expected to react faster than CO_2, leading to hydrocarbons that do not originate from the actual photocatalytic process facilitated by the tested material.

Furthermore, a photocatalytic CO_2 reduction experiment can be performed either in batch or in flow-through mode [35]. On the one hand, flow conditions lead to faster reaction rates. However, since the concentration of even the major photocatalytic CO_2 reduction products are quite low, it is very difficult to identify and accurately quantify them during flow-through conditions. On the other hand, a batch mode process allows for a more accurate estimation of the products' yields even at lower concentrations, as the amount of molecules accumulate over the total reaction time. Besides the use of H_2O, both in liquid- and gas-phase, the CO_2 photoconversion into CH_4 can also be carried out by mediating hydrogen at room temperature and atmospheric pressure called photo-methanation [36]. Furthermore, literature concerning the effect of Ag oxidation state on CO_2 photoreduction activities is rarely studied. Most of the research on CO_2 photoreduction only focuses on the effect of the Ag metallic co-catalyst which contributes through the electron trapping and LSPR mechanism [33,37].

In this study, Ag nanoparticles were deposited on commercial TiO_2 (anatase) using the liquid impregnation method. This method was employed as it is simple, fast, and of low cost [38,39]. The physical and chemical properties of the synthesized Ag/TiO_2 composites were extensively

studied and characterized using X-ray powder diffraction (XRD), scanning electron microscopy (SEM), ultra violet-visible (UV-Vis) spectrophotometry, X-ray photoelectron spectroscopy (XPS), and transmission electron microscopy (TEM). Furthermore, the assessment of the photocatalytic CO_2 reduction activity of the aforementioned materials, the study of the influence of Ag loading, and the effect of mixed Ag species and the LSPR on the products' concentration was carried out in a high purity gas-phase photoreactor.

2. Results and Discussion

2.1. Synthesis of Photocatalysts

All investigated Ag/TiO_2 materials have been successfully prepared by facile impregnation methods. Commercially available TiO_2 (anatase, $\geq$99.0%, Merck) was used in this study, both as a starting and as a reference material. The Ag decorated TiO_2 photocatalysts were prepared using a modified liquid impregnation method [14]. The resulting Ag modified TiO_2 photocatalysts were referred to as $Ag/TiO_2X\%$ (X = 1–4), whereby X is the nominal silver loading.

2.2. Characterization of Photocatalysts

2.2.1. Powder X-ray Diffraction

X-ray diffraction techniques were used to determine crystallinity and structural changes which may occur during Ag metal deposition. Figure 1 shows the XRD powder patterns of the pristine TiO_2 and the various Ag/TiO_2 samples calcined at 500 °C in air atmosphere. As depicted, all prepared materials exhibited high crystallinity. There were no detectable changes in the crystal structure of the materials during Ag deposition. All materials retained the tetragonal crystal structure of TiO_2 anatase. The main reflexes at $2\theta\sim25°$, $38°$, and $48°$ were attributed to the (101), (004), and (200) planes of TiO_2 anatase (JCPDS File No. 83-2243), respectively. For Ag/TiO_2 materials, small reflexes at $2\theta\sim44°$ indicated the presence of Ag^0 species with a lattice plane of (200) (JCPDS File No. 04-0783). The emergence of Ag^0 species is due to the partial reduction of Ag^+ ($AgNO_3$) under high temperature conditions used in the synthetic protocol. The reflex characteristic of the Ag^0 species can be clearly seen for the 2%, 3%, and 4% Ag/TiO_2 composites. Furthermore, there were also small reflexes ($2\theta\sim33.2°$) which corresponded to the diffraction pattern of (111) planes of Ag_2O species (JCPDS File No. 41-1104). In addition, it can be assumed that Ag was not incorporated into the TiO_2 structure, but deposited on its surface (vide infra) [11].

From the powder XRD data it can be concluded that the as-synthesized materials contained a mixture of Ag^0 and Ag^I species, and that the Ag was not completely reduced to Ag^0 during the synthesis. This phenomenon occurs due to the calcination in air atmosphere, where O_2 inhibits the complete reduction of all Ag species. The calcination process at 500 °C decomposes $AgNO_3$ into different Ag species, NO_x gas, and O_2 gas.

The average crystallite size of deposited Ag for each sample was calculated from the broadening of the cubic Ag (200) reflex using the Scherrer equation (Equation (1)):

$$D = \frac{0.94\,\lambda}{\beta_{1/2}\cos\theta} \tag{1}$$

where D is the crystallite size, λ is the X-ray wavelength used in this analysis, $\beta_{1/2}$ is the full width at half maximum, and θ is the main reflex of XRD pattern. Based on this calculation, the size of deposited Ag nanoparticles varies from 28 nm to 37 nm ($Ag/TiO_24\%$ exhibited the largest crystallite size among the tested samples). Further SEM and TEM analyses were used to support these data (see Figures 5 and 6).
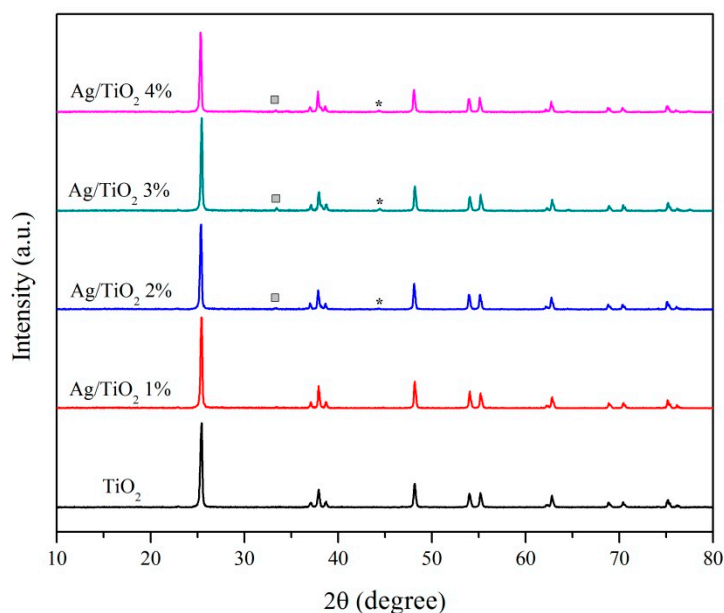
Figure 1. Powder XRD patterns of pristine TiO_2 and Ag/TiO_2 materials. Small squares (□) at $2\theta = 33.2°$ indicate the presence of Ag^I species and the small stars (*) at $2\theta = 44.4°$ indicate the presence of Ag^0.

2.2.2. Electronic Spectra

To study the optical properties and light absorption effects of Ag species deposited on TiO_2, UV-Vis spectra were collected from the tested samples in a pressed disk form. Figure 2a demonstrates the absorption properties of the as-synthesized materials in the wavelength range 250–800 nm. As it is clearly seen, the reference TiO_2 sample has only UV light absorption. The deposited Ag species contributed to an increase in the material's absorption towards the visible region as seen in the 420–700 nm wavelength range (see inset graph). This is in accordance with previous work on visible light absorption in Ag nanoparticles species at 410–425 nm due to the surface plasmon resonance effect [40–46] (Figure 2b). The absorption, with a maximum near 425 nm, can be attributed to the plasmon absorption of spherical Ag nanoparticles [45], whereas the broad absorption reaching down to ~700 nm may be attributed to differently shaped Ag nanoparticles, such as cube-like structures [45], or to the absorption of Ag_2O [47].


(**a**)

Figure 2. *Cont.*

(**b**)
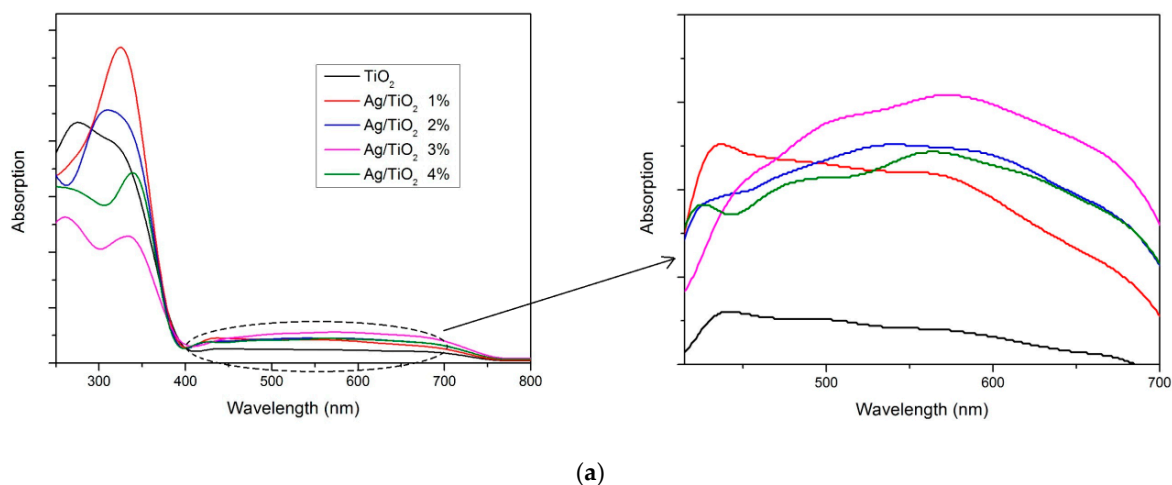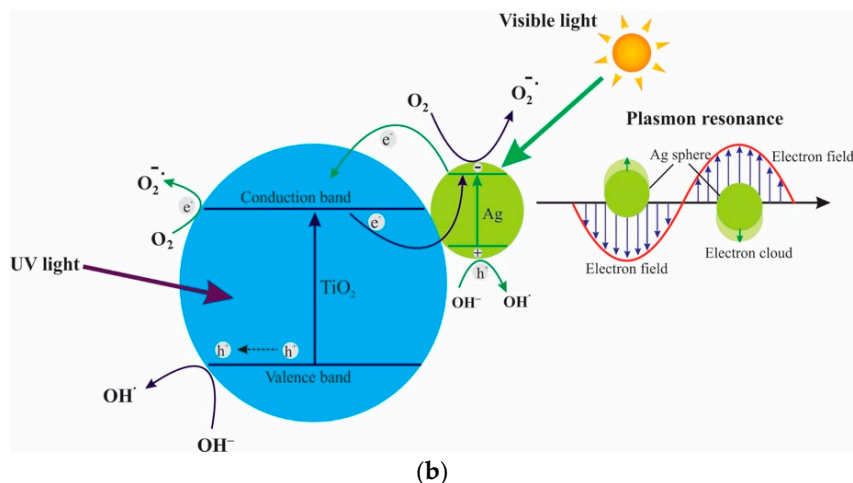
Figure 2. (**a**) UV-Visible spectra of TiO_2 and Ag/TiO_2 as pressed disks. Inset shows the material absorption magnification at 400–700 n; (**b**) surface plasmon resonance (SPR) effect of Ag species deposited on TiO_2 surface, modified from reference [48].

In order to further investigate the electronic properties of the Ag/TiO_2 materials, additional UV-Vis diffuse reflectance spectra were collected for all samples. To this aim, the Kubelka–Munk function, F(R), allows the optical absorbance of the materials to be approximated from their reflectance (R) according to [49] (Figure 3a). The band gap energy of the tested samples can be estimated from the Tauc plot, using equations from the literature [50].
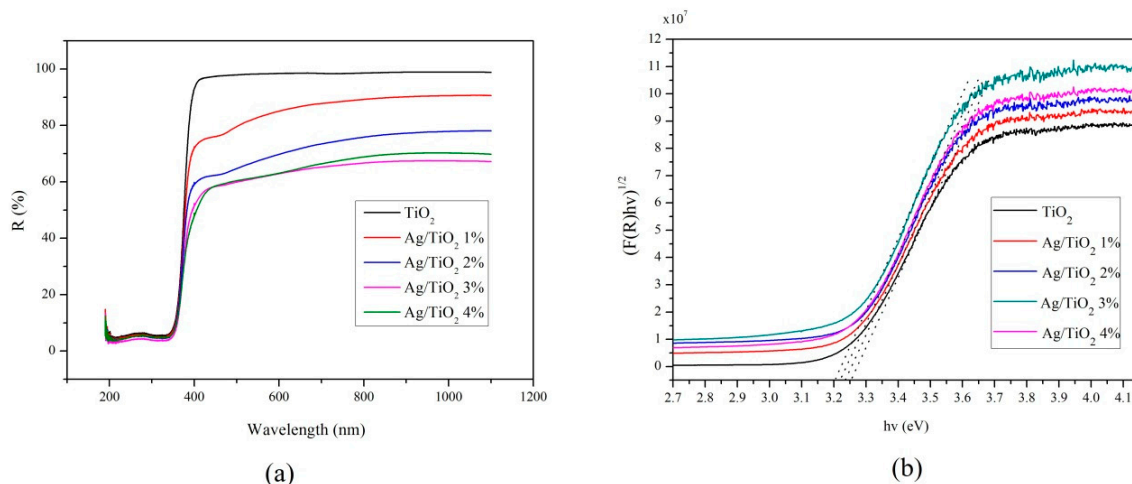

Figure 3. (**a**) Diffuse reflectance spectra and (**b**) band gap calculation of TiO_2 and $Ag/TiO_2X\%$ (X = 1–4).

The optical band gap energy calculation was determined by extrapolating the linear region of the plot hv vs $(F(R)hv)^{1/2}$ as shown in Figure 3b. The calculation shows that the band gap energy of the prepared materials is in the 3.15–3.20 eV range. This slight shift indicates that the deposition of Ag (1%–4%) on the surface of TiO_2 does not significantly affect the band gap energy.

2.2.3. Determination and Characterization of Surface Ag on TiO_2

X-ray photoelectron spectroscopy was implemented to investigate the surface chemical state and composition of the as-prepared samples. Figure 4a shows the survey spectrum of the 4% Ag/TiO_2 sample. From the area Ag 3d and Ti 2p photoelectron peaks, and respective sensitivity factors, the surface Ag:Ti atomic percentage was estimated to be 20%. The positive deviation respect to the nominal Ag:Ti ratio suggests that Ag particles are indeed decorating the TiO_2 surface—photoelectron

spectroscopy is largely surface sensitive where the Ag is located. Besides the peak from Ti, O, and Ag, traces of C (C 1s) can be detected. This is usually ascribed either to carbon impurities in the titania, or to adventitious carbon during the XPS measurement.
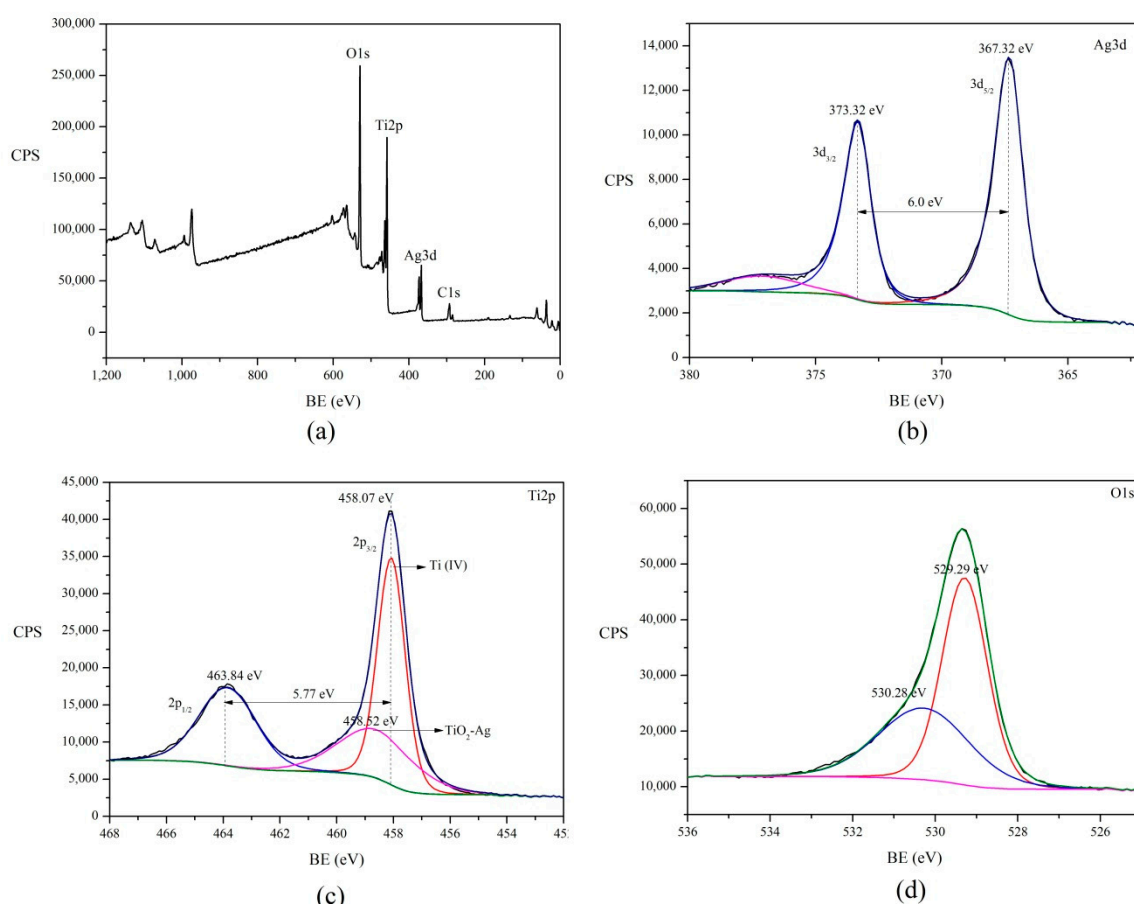
Figure 4. X-ray photoelectron (XP) spectra of Ag/TiO_2 4%: (**a**) Survey scan spectrum and peak fitting results of (**b**) Ag 3d, (**c**) Ti 2p, and (**d**) O 1s.

From the high-resolution X-ray photoelectron (XP) spectrum of Ag 3d (Figure 4b), the binding energy (BE) corresponding to the Ag $3d_{5/2}$ peak appears at 367.32 eV. In addition, the BE of Ag $3d_{3/2}$ is located at 373.32 eV. Those two peaks indicate the formation of Ag^I species [51]. The peak is asymmetric and broad and therefore it is designated to two Ag species (Ag^I and metallic Ag). This is in accordance with results from XRD measurements (see above). The asymmetry and broadness disappears in fully reduced samples where metallic Ag is present only. Furthermore, it is noteworthy, that XPS also detected the presence of potassium most probably originating from impurities contained in the precursors used in the synthesis of the materials. The shoulder at high BE in the Ag 3d region is assigned to K 2s. This impurity may contribute to the low photochemical activity because this is known for the comparable impact of sodium in CO_2 reduction (see below) [34].

Figure 4c illustrates the Ti 2p spectrum of the same Ag/TiO_2 4% sample. The peak for Ti $2p_{3/2}$ can be fitted with two components, one located at 458.07 eV and the other at 458.62 eV. Both peaks are attributed to Ti^{IV}. The small positive shift (ca. 0.6 eV) is due to the strong interaction between TiO_2 and Ag species leading to electron transfer from the former to the latter [52,53]. Another peak located at 463.83 eV is assigned to Ti $2p_{1/2}$. The splitting between Ti $2p_{3/2}$ and Ti $2p_{1/2}$ is 5.75 eV indicates that Ti exists as Ti^{IV} species [54]. Meanwhile, no shoulder peaks at BE 462.5 eV and 456.8 eV for Ti $2p_{1/2}$ and Ti $2p_{3/2}$ core level of Ti^{III} appear, indicating that no Ti^{III} species exist on the surface of the material [55].

Figure 4d depicts the fitting of the O 1s peak. An asymmetric peak of O 1s can be deconvoluted into two peaks. These peaks are located at 529.29 eV and 530.28 eV corresponding to the Ti–O [56] and H–O bonds [57], respectively. All those peaks are corresponding to O^{2-} species.

2.2.4. Electron Microscopy and Energy-Dispersive X-ray Spectroscopy

In order to investigate the surface morphology of the samples, SEM pictures were collected (Figure 5). No significant morphology differences between the pure TiO_2 anatase and the Ag/TiO_2 can be found (not shown). SEM results show agglomerated spherical TiO_2 particles with crystallite diameters in the 100–200 nm range. From Figure 5 it can be clearly seen that the Ag nanoparticles emerge (appearing as white bright spheres) on the surface of TiO_2. The size of the Ag nanoparticles varies from 2–50 nm. It is in accordance with calculations from the powder XRD data (see above). The energy dispersive X-ray (EDX) analysis confirmed that the actual Ag loading is 1.1%, 1.8%, 2.1%, and 3.6% for Ag/TiO_2 1%, Ag/TiO_2 2%, Ag/TiO_2 3%, and Ag/TiO_2 4%, respectively. Small deviations between nominal and actual loading may be due to the uneven distribution of the Ag nanoparticles on the surface of the $Ag-TiO_2$ composite.
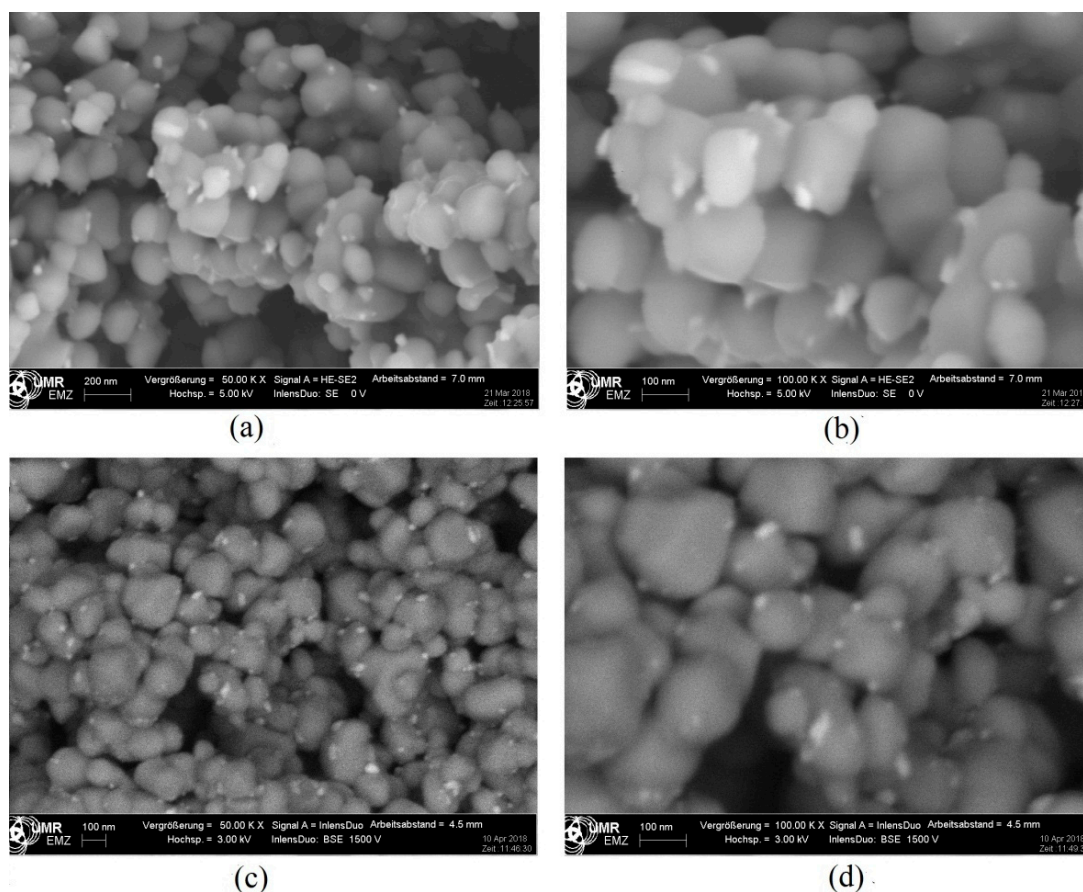
Figure 5. SEM images of Ag/TiO_2 4% in (**a**) 50,000 and (**b**) 100,000 magnifications (backscaterred electron (BSE) detector used for images (**c**) and (**d**)).

TEM images of the 2% and 4% Ag/TiO_2 are shown in Figure 6. As shown in Figure 6a,b, Ag (appearing as small dark spheres) is distributed unevenly on the TiO_2 covering only selected areas of the TiO_2 surface, which is in accordance with previous research [22]. Furthermore, the size distribution of Ag nanoparticles also varies as seen from Figure 6c. From the TEM images (Figure 6c–e) the lattice fringes allow the identification of crystallographic spacing. The d-spacing value of 0.35 nm corresponds to the anatase (101) plane [57,58], whereas the d values of 0.28 nm and 0.16 nm, respectively, represent

the plane of (111) and (220) for Ag_2O species [59–61]. These results strongly support the results from powder X-ray diffraction (see above).
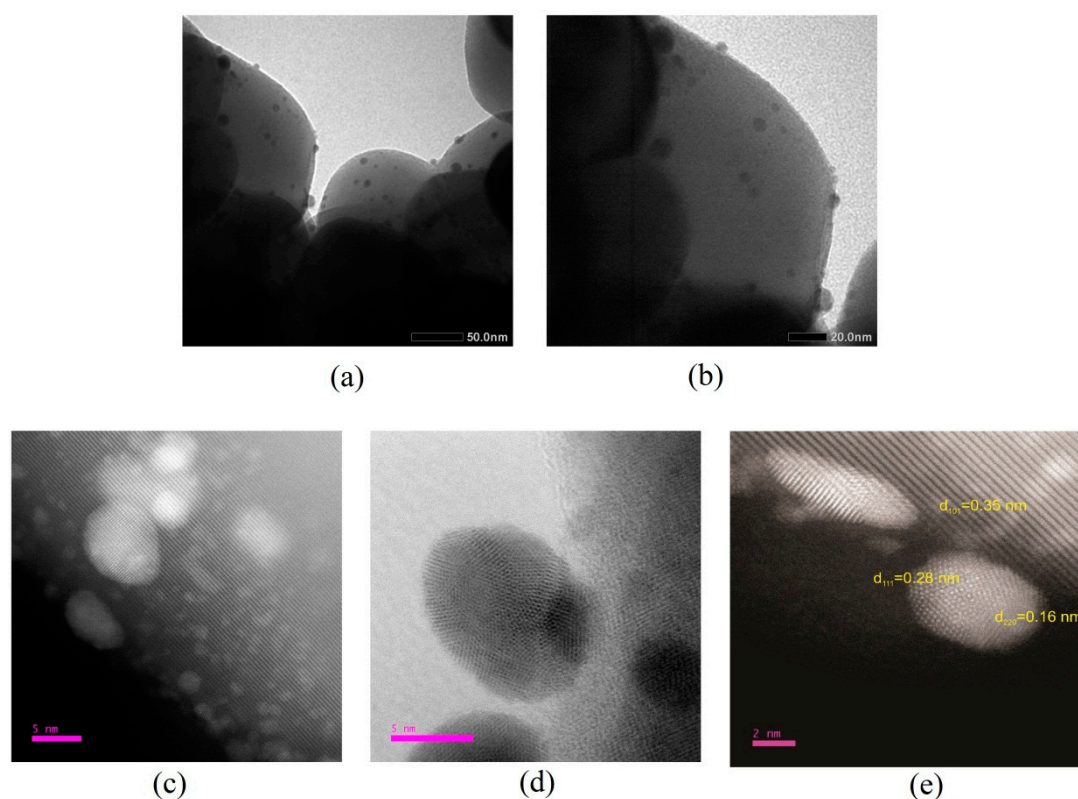
Figure 6. TEM images of Ag/TiO_2 2% (**a,b**) and TEM images of Ag/TiO_2 4% (**c–e**).

2.3. Photocatalytic Activity in CO_2 Reduction

Sample Testing in Photocatalytic CO_2 Reduction

As carbon-containing impurities adsorbed onto the surface of the photocatalysts can lead to overestimation of the concentration of the products of CO_2 reduction, special attention must be paid to sufficiently remove them. These impurities might originate from the synthesis process (from precursors, solvents, etc.) or from adsorbed species (e.g., atmospheric CO_2 and hydrocarbons). As explained in detail in the experimental section, extensive cleaning of the materials in a gas-phase of only water in inert gas was performed. This cleaning approach usually ensures that impurities are sufficiently removed and that the observed products in photocatalytic CO_2 reduction originate predominantly from true photocatalytic reaction between both H_2O and CO_2. However, this is not the case here. All four Ag loaded samples were tested under conditions of high-purity in photocatalytic CO_2 reduction and compared to the reference TiO_2 material. Only in the case of Ag/TiO_2 2% was a CH_4 production not originating from residual C-containing impurities identified. In all other samples (Ag/TiO_2 1%, 3%, and 4% and reference TiO_2), the levels of CH_4 produced in the cleaning procedure (i.e., in absence of CO_2) and in the actual reaction with CO_2 and H_2O in the gas-phase were identical (not shown). So, for all samples except Ag/TiO_2 2%, CH_4 formation can be attributed solely to left-over impurities. Consequently, only Ag/TiO_2 2% is further considered in comparison with the reference TiO_2 (Figure 7).

It is remarkable that the reference TiO_2 used in this work was almost inactive in photocatalytic CO_2 reduction (Figure 7), although a broad-band 200 W Hg/Xe light source was used that was able to excite TiO_2. Not only was the CH_4 yield very low (~1.2 ppm), it was also identical in the cleaning procedure and the CO_2 reduction experiment. The low to non-existent activity may have to do with TiO_2 being present only in anatase structure, because usually P25 with both rutile and anatase

components (~80/20%) is used and shows high activity [32,34,35,62]. Furthermore, the titania may be highly defective, so that recombination events are predominant. While we cannot clearly give an answer to the inactivity of the reference TiO_2, it is obvious that the presence of Ag induces photocatalytic activity, the origin of which is further studied.
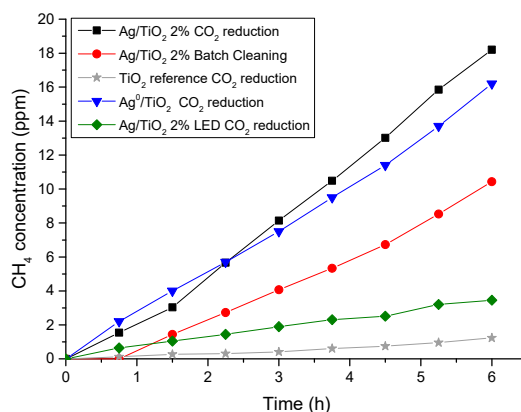
Figure 7. CH_4 concentration over time for the Ag/TiO_2 2% sample in batch cleaning, and CO_2 reduction with Hg/Xe lamp and LED, as well as CO_2 reduction with metallic state Ag^0/TiO_2 2%. Bare TiO_2 is used as a reference.

The 2% Ag loaded sample exhibited considerably higher CH_4 production compared to the bare anatase reference TiO_2 (Figure 7). Furthermore, almost twice as much CH_4 was formed, as in the case of the cleaning procedure, so at least half of all products must originate from CO_2 as carbon source. The higher photocatalytic efficiency of the Ag decorated TiO_2 sample is often attributed to the fact that the Ag species act as electron scavengers and therefore the recombination of the photo-generated $e^- - h^+$ pairs is hindered [63]. The photo-generated electron transfer from the TiO_2 conduction band to the Ag species deposited on the surface is thermodynamically possible due to the higher Fermi energy level of TiO_2 compared to Ag [64]. As a result, the formation of a Schottky barrier occurs at the interface between Ag and TiO_2, which can further improve the charge separation and consequently, the photocatalytic activity [65]. The Schottky barrier prevents the back-transfer of electrons from Ag to TiO_2, thus they remain trapped in the Ag species. Since the titania itself is inactive in the present work, two explanations may account for the improved activity of the Ag/TiO_2 sample: Either recombination in the bare titania is so much favored that charge separation is only possible in presence of Ag, or titania contributes nothing to the observed photoactivity, because it is only due to the localized surface plasmon resonance (LSPR) effect. The LSPR effect induced by the presence of Ag nanoparticles in the visible region can boost the energy of trapped electrons through the strong local electron field of LSPR, making it react with electron acceptors more easily [28]. This synergistic effect of the LSPR effect and the $e^- - h^+$ separation can lead to an enhancement in the photocatalytic activity as shown in Figure 2b.

In order to test how the LSPR effect influences the CH_4 production, a CO_2 reduction experiment was performed with the Ag/TiO_2 2% sample, using a 10 W 365 nm high-power LED while all the other experimental parameters remained the same. As it can be seen from Figure 7, the CH_4 concentration is much higher when the Hg/Xe lamp (containing wavelengths in both UV and visible range of the light spectrum) was used compared to the CH_4 production under LED illumination. This means that the absorption of the Ag/TiO_2 2% sample in the 420–550 nm range due to the LSPR effect is the main reason for the observed photocatalytic activity of this sample.

The observation of favorable performance of a sample with ~2 wt % Ag is in a good agreement with Zhao et al. [37]. They reported that the optimal Ag concentration on TiO_2 was 2 wt % in simultaneous H_2 production and photocatalytic CO_2 reduction. Similar results were also obtained by Liu et al. [28] and Yu et al. [30]. Based on Liu et al. the composite of 2.5% Ag/TiO_2 exhibits the best activity in CO_2 reduction compared with other Ag loadings. On the other hand, Yu et al. proposed

that 1.5% Ag/TiO_2 is the best material. This is due to the further increase of Ag loading triggering the LSPR peak to become slightly red-shifted and broader, implying that the Ag nanoparticles begin to agglomerate. However, the exact CH_4 production rate for those studies was different due to the difference of both material properties and reactor set up.

Additionally, it must be clarified which oxidation state of Ag is required for high photoactivity. In order to study the effect of the Ag oxidation state, a sample in which all Ag has been reduced to the metallic state (namely Ag^0/TiO_2 2%) was tested in CO_2 reduction under similar conditions as the Ag/TiO_2 2%, which contained both Ag^0 and Ag^I. As it can be seen from Figure 7, a mixed oxidation state is photocatalytically beneficial. One explanation for this higher photocatalytic activity may be the presence of a Ag_2O–TiO_2 interface that may act as an e$^-$ trapping layer compared to the pure Ag^0 loaded sample. As reported in [66] an interfacial charge transfer (IFCT) takes place between Ag_2O and TiO_2 under band gap irradiation. This is facilitated by the position of the energy bands of Ag_2O and TiO_2, as the conduction band of Ag_2O is more negative than that of TiO_2. This electron transfer hinders the e$^-$–h$^+$ recombination in the Ag_2O. The photo-produced h$^+$ reacts with H_2O generating OH$^\circ$ and H$^+$.

Furthermore, considering the function of the Ag^0/Ag^I species as a co-catalyst, mixed systems composed of a metallic core and an oxide shell have often been found beneficial for different reactions. For example, a Ni/NiO core shell system, as well as Rh/Cr_2O_3 or CuO_x/Cr_2O_3 systems (in which the core-shell structure is debated) have been found beneficial for water splitting, particularly for hydrogen evolution [67–70]. While the metal ensures a conducting contact with the semiconductor and may act as the catalytic active site for reduction [70], the oxide (shell) may have other functions, such as prevention of the back reaction or functioning for water oxidation [67,71]. Although the structural arrangement of the Ag^0 and Ag^I (core-shell, neighboring, far from each other, etc.) is not known in the present case, it is possible that both species adopt important roles in the mechanism. We can only speculate that electron conduction and electron pooling may proceed on Ag^0, whereas adsorption of CO_2 or stabilization of some relevant intermediates may take place on Ag^I. This needs to be clarified in future studies.

Since a general mechanism for photocatalytic CO_2 reduction is not yet clear, an a priori design of a suitable catalyst is not an easy task. However, TiO_2-based materials with co-catalysts (mixed states, metal loaded, z-schemes, etc.) have the potential to exhibit good efficiencies in producing useful chemicals from CO_2. The optimum synthesis parameters should be optimized both in terms of efficiency, but also in terms of cost, environmental burden, and sustainability. The necessity for high purity experimental conditions is eminent in combination with (at least) blank experiments in order to reach safer conclusions about novel materials.

3. Experimental Section

3.1. General Considerations

Powder XRD data were obtained on a Miniflex 600 device (Rigaku, Tokyo, Japan) in the range of $2\theta = 3$–$80°$ (0.2° step, 30 kV, 10 mA, Cu K_α). UV-Vis spectra were recorded on a UV-2450PC PharmaSpec device (Shimadzu, Kyoto, Japan) for dry-pressed sample disks and on a Lambda 365 device (PerkinElmer, Waltham, MA, USA) in the diffuse reflectance mode for the as-synthesized powders, respectively. XPS data were recorded on a K-Alpha device (ThermoFisher Scientific, Waltham, MA, USA) using a 72 W monochromated Al K_α source. All XP spectra were referenced according to the C 1 s peak at 285 eV. Simulations of the experimental photopeaks were carried out using a mixed Gaussian/Lorentzian peak fit procedure according to the CasaXPS software. Semi-quantitative analysis accounted for a nonlinear Shirley background subtraction. SEM measurements were done using a Merlin VP compact device (Zeiss, Oberkochen, Germany) and additional EDX investigations were performed using a Quantax 400 device (Bruker, Billerica, MA, USA). TEM images were recorded either on a JEM-1400 device (Jeol, Akishima, Japan), or on a JEM-ARM200F device (Jeol, Akishima,

Japan). Gas chromatograph (GC) measurements during photocatalytic CO_2 reduction were collected using a Tracera GC-2010 Plus device (Shimadzu, Berlin, Germany) equipped with a barrier ionization discharge detector (BID) and a flame ionization detector (FID).

3.2. Materials

All starting materials were purchased commercially from Merck and used as received: Titania TiO_2 (anatase, $\geq$99.0%), silver nitrate ($AgNO_3$, $\geq$99.0%).

3.3. Preparation of Photocatalysts

The Ag decorated TiO_2 photocatalysts were prepared using a liquid impregnation method, which is exemplified in the following for the 1 mol% Ag/TiO_2 sample. TiO_2 powder (7.99 g) and 0.17 g of $AgNO_3$ precursor were added in 100 mL of distilled water. The theoretical loading amount of Ag was 1 mol% (the molar ratio of Ag to TiO_2). The slurry was kept under stirring and heated at 80 °C for 4 h to achieve Ag^+ equilibrium on the surface of TiO_2. The stirring process was equipped with reflux apparatus. Then, the slurry was allowed to settle at room temperature overnight. The formed slurry was dried in an oven for 12 h at a temperature of 100 °C. The resulting solid was ground with a mortar and subsequently calcined at 500 °C for 3 h in air. For the preparation of the samples with different Ag loadings, the amount of $AgNO_3$ was varied accordingly, while all other reagent amounts were kept similar. The resulting Ag modified TiO_2 photocatalysts are referred to as Ag/TiO_2X% (X = 1–4) [30]. The Ag^0/TiO_2 2% composite was prepared by reducing the Ag/TiO_2 2% sample using 20% H_2 (in Ar) for 1 h at 200 °C.

3.4. Photocatalytic Setup

The photocatalytic CO_2 reduction experiments were carried out in a high-purity gas-phase photoreactor setup. A detailed description of the photocatalytic reactor design was given by Mei et al. [6]. In brief, the photoreactor is made exclusively of stainless steel components suitable for ultra-high vacuum applications. All of the tube connections were realized using vacuum coupling radiation (VCR) fittings, thus ensuring a grease-free sealing of all interconnecting parts. The sample powder was spread as evenly as possible on a quartz sample holder (diameter ~2.5 cm) placed in the center of the photoreactor. High purity He (6.0) and 1.5% CO_2/He (5.5/6.0) mixture were used in the experiments and their respective flows towards the reactor were adjusted using a set of two mass flow controllers (MFC). Water enrichment of the gas mixtures was performed in a temperature-controlled stainless-steel saturator. All water-carrying pipes were constantly heated to 120 °C to avoid internal H_2O condensation. A 200 W Hg/Xe lamp (Newport Oriel) emitting UV and visible light was used as the irradiation source, as well as a 10 W array of 4 high-power LEDs emitting at 365 nm (SeoulVioSys). A water-based filter was used for IR radiation removal from the lamp to avoid sample heating. The product analysis was performed using a Shimadzu Tracera GC 2010 plus gas chromatograph (GC) equipped with a barrier ionization discharge detector (BID—Q Bond 50 m column 5A molecular sieve) and a flame ionization detector (FID—Alumina Bond/KCl 50 m column). Helium (He) at a flow of 25 mL min^{-1} was used as the carrier gas in the GC. The temperature of the columns was increased from initially 30 °C up to finally 160 °C (heating rate: 20 °C min^{-1}). Then the temperature was decreased back to 30 °C (cooling rate: 50 °C min^{-1}) and immediately afterwards increased again to 160 °C (heating rate: 20 °C min^{-1}). In total, 33 min were needed for a complete measurement with a 5-min cool-down period. This procedure facilitated desorption of molecules from the column.

3.5. Sample Pretreatment

Before studying the performance of the samples in photocatalytic CO_2 reduction, extensive cleaning was performed to clean the materials' surface from residual carbon-containing species. These impurities can react with CO_2 and H_2O molecules to form hydrocarbons, thus leading to overestimation of the efficiency of the materials towards CO_2 reduction. The cleaning process applied involved two

steps: In the first step, the samples were re-calcined at 400 °C for 3 h at a rate of 180 K h^{-1} under a synthetic air environment to remove the majority of the adsorbed C-containing impurities. In the second step, the cleaning process continued with the sample (50 mg) inside the photoreactor in batch mode. The reactor was filled with H_2O (T_{H2O} = 5 °C)-saturated pure He (at a flow of 10 mL min^{-1}) up to a final pressure of 1500 mbar. A gas sample was collected every 45 min from the batch reactor, for a total duration of 6 h, with the first chromatogram taken without light irradiation. As with each collected sample, when the pressure inside the reactor dropped, a pressure-based correction was performed. Subsequently, a flow-through cleaning process took place, where moist pure He flowed continuously (at a rate of 20 mL min^{-1}) over the sample under light irradiation for 3 h. Under these circumstances, detection of products from sample cleaning was not accurately possible, so the flow cleaning was followed by a second batch cleaning process. The amount of CH_4 produced from impurities in this second batch cleaning were compared to CH_4 formation in the photocatalytic CO_2 reduction experiment in order to evaluate the relative number of products truly originating from CO_2.

3.6. Photocatalytic CO_2 Reduction

The photocatalytic CO_2 reduction experiment was carried out in batch mode conditions. The experimental conditions and GC analysis were similar to the batch cleaning process, except for the presence of CO_2 as a reactant gas. Thus, the gas-phase feed of the reactor consisted of 1.5% CO_2 diluted in He and saturated with H_2O at 5 °C. The product analysis was also performed every 45 min with the necessary pressure drop corrections. An extensive set of blank measurements (no photocatalyst, no CO_2, no light, and combinations of the above) were performed to ensure that no, or sufficiently low, concentration of hydrocarbons were produced at conditions other than a CO_2 reduction experiment.

4. Conclusions

In this study, Ag nanoparticles deposited on commercial anatase TiO_2 were successfully prepared by liquid impregnation method. As XPS analysis results indicated, the composite contained the mixture of Ag^I and Ag^0 on the surface of TiO_2. It was found that all silver/titania materials had visible light absorption due to surface plasmon absorption of electrons in silver species. The TEM and SEM images showed the uneven dispersion of Ag nanoparticles with a diameter of ~2–50 nm on the TiO_2 surface. Only the sample with 2 wt % Ag was revealed to be an effective material for CO_2 reduction. The LSPR effect was studied using two different irradiation sources containing only UV (365 nm LED) or both UV and visible (Hg/Xe lamp) wavelengths, and it was identified as the main reason for the photocatalytic activity of the Ag/TiO_2 2% sample. In addition, the presence of mixed-valent silver was beneficial for CH_4 formation in photocatalytic CO_2 reduction. A sample in which all silver has been reduced to the metallic state was instead less active.

Author Contributions: Conceptualization, C.T.H., N.G.M., and T.P.; methodology, C.T.H., N.G.M., T.P., F.E.O., and A.S.; validation, N.G.M., T.P., J.S., M.D.B., B.Y., and F.G.; formal analysis, C.T.H., N.G.M., T.P., F.E.O., A.S., M.D.B, and B.Y.; investigation, C.T.H., N.G.M., T.P., F.E.O., A.S., and A.H.; writing—original draft preparation, C.T.H., N.G.M., T.P., and A.H.; writing—review and editing, N.G.M., T.P., J.S., and F.G.; visualization, C.T.H., N.G.M., T.P., F.E.O., and A.S.; supervision, J.S., and F.G.; project administration, J.S., T.P., and F.G.

References

1. Low, J.; Cheng, B.; Yu, J. Surface modification and enhanced photocatalytic CO_2 reduction performance of TiO_2: A review. *Appl. Surf. Sci.* **2017**, *392*, 658–686. [CrossRef]

2. NASA. Climate Change Vital Signs of the Planet: Carbon Dioxide. Available online: https://climate.nasa.gov/vital-signs/carbon-dioxide/ (accessed on 6 March 2018).

3. NASA. Global Climate Change Vital Signs of the Planet: Global Temperature. Available online: https://climate.nasa.gov/vital-signs/global-temperature/ (accessed on 6 March 2018).

4. Jiang, Z.; Xiao, T.; Kuznetsov, V.L.; Edwards, P.P. Turning carbon dioxide into fuel. *Philos. Trans. A Math. Phys. Eng. Sci.* **2010**, *368*, 3343–3364. [CrossRef]

5. Ji, Y.; Luo, Y. New mechanism for photocatalytic reduction of CO_2 on the anatase TiO_2 (101) surface: The essential role of oxygen vacancy. *J. Am. Chem. Soc.* **2016**, *138*, 15896–15902. [CrossRef]

6. Mei, B.; Pougin, A.; Strunk, J. Influence of photodeposited gold nanoparticles on the photocatalytic activity of titanate species in the reduction of CO_2 to hydrocarbons. *J. Catal.* **2013**, *306*, 184–189. [CrossRef]

7. Li, K.; An, X.; Park, K.H.; Khraisheh, M.; Tang, J. A critical review of CO_2 photoconversion: Catalysts and reactors. *Catal. Today* **2014**, *224*, 3–12. [CrossRef]

8. Handoko, A.D.; Li, K.; Tang, J. Recent progress in artificial photosynthesis: CO_2 photoreduction to valuable chemicals in a heterogeneous system. *Curr. Opin. Chem. Eng.* **2012**, *2*, 200–206. [CrossRef]

9. Yuan, L.; Xu, Y.-J. Photocatalytic conversion of CO_2 into value-added and renewable fuels. *Appl. Surf. Sci.* **2015**, *342*, 154–167. [CrossRef]

10. Sato, S.; Arai, T.; Morikawa, T. Toward solar-driven photocatalytic CO_2 reduction using water as an electron donor. *Inorg. Chem.* **2015**, *54*, 5105–5113. [CrossRef]

11. Zhao, B.; Chen, Y.-W. Ag/TiO_2 sol prepared by a sol–gel method and its photocatalytic activity. *J. Phys. Chem. Solids* **2011**, *72*, 1312–1318. [CrossRef]

12. Lai, Y.; Chen, Y.; Zhuang, H.; Lin, C. A facile method for synthesis of Ag/TiO_2 nanostructures. *Mater. Lett.* **2008**, *62*, 3688–3690. [CrossRef]

13. Li, X.; Wen, J.; Low, J.; Fang, Y.; Yu, J. Design and fabrication of semiconductor photocatalyst for photocatalytic reduction of CO_2 to solar fuel. *Sci. China Mater.* **2014**, *57*, 70–100. [CrossRef]

14. Saha, S.; Wang, J.M.; Pal, A. Nano silver impregnation on commercial TiO_2 and a comparative photocatalytic account to degrade malachite green. *Sep. Purif. Technol.* **2012**, *89*, 147–159. [CrossRef]

15. Etacheri, V.; Valentin, C.D.; Schneider, J.; Bahnemann, D.; Pillai, S.C. Visible-light activation of TiO_2 photocatalysts: Advances in theory and experiments. *J. Photochem. Photobiol. C* **2015**, *25*, 1–83. [CrossRef]

16. Schneider, J.; Matsuoka, M.; Takeuchi, M.; Zhang, J.; Horiuchi, Y.; Anpo, M.; Bahnemann, D.W. Understanding TiO_2 Photocatalysis: Mechanisms and Materials. *Chem. Rev.* **2014**, *114*, 9919–9986. [CrossRef] [PubMed]

17. Ablat, A.; Wu, R.; Mamat, M.; Ghupur, Y.; Aimidula, A.; Bake, M.A.; Gholam, T.; Wang, J.; Qian, H.; Wu, R.; et al. Electronic structure and room temperature ferromagnetism of C doped TiO_2. *Solid State Commun.* **2016**, *243*, 7–11. [CrossRef]

18. Kočí, K.; Matějová, L.; Ambrožová, N.; Šihor, M.; Troppová, I.; Čapek, L.; Kotarba, A.; Kustrowski, P.; Hospodková, A.; Obalová, L. Optimization of cerium doping of TiO_2 for photocatalytic reduction of CO_2 and photocatalytic decomposition of N_2O. *J. Sol-Gel Sci. Technol.* **2016**, *78*, 550–558. [CrossRef]

19. Rho, W.-Y.; Jeon, H.; Kim, H.-S.; Chung, W.-J.; Suh, J.S.; Jun, B.-H. Recent progress in dye-sensitized solar cells for improving efficiency: TiO_2 nanotube arrays in active layer. *J. Nanomater.* **2015**, *2015*, 1–17. [CrossRef]

20. Wang, T.; Xia, M.; Kong, X. The pros and cons of polydopamine-sensitized titanium oxide for the photoreduction of CO_2. *Catalysts* **2018**, *8*, 215. [CrossRef]

21. Yoon, J.-W.; Sasaki, T.; Koshizaki, N.; Traversa, E. Preparation and characterization of M/TiO_2 (M = Ag, Au, Pt) nanocomposite thin films. *Scripta Mater.* **2001**, *44*, 1865–1868. [CrossRef]

22. Kim, K.D.; Han, D.N.; Lee, J.B.; Kim, H.T. Formation and characterization of Ag-deposited TiO_2 nanoparticles by chemical reduction method. *Scripta Mater.* **2006**, *54*, 143–146. [CrossRef]

23. Tahir, K.; Ahmad, A.; Li, B.; Khan, A.U.; Nazir, S.; Khan, S.; Khan, Z.U.H.; Khan, S.U. Preparation, characterization and an efficient photocatalytic activity of Au/TiO_2 nanocomposite prepared by green deposition method. *Mater. Lett.* **2016**, *178*, 56–59. [CrossRef]

24. Dozzi, M.V.; Brocato, S.; Marra, G.; Tozzola, G.; Meda, L.; Selli, E. Aqueous ammonia abatement on Pt- and Ru-modified TiO_2: Selectivity effects of the metal nanoparticles deposition method. *Catal. Today* **2017**, *287*, 148–154. [CrossRef]

25. Olivo, A.; Ghedini, E.; Pascalicchio, P.; Manzoli, M.; Cruciani, G.; Signoretto, M. Sustainable carbon dioxide photoreduction by a cooperative effect of reactor design and titania metal promotion. *Catalysts* **2018**, *8*, 41. [CrossRef]

26. Mital, G.S.; Manoj, T. A review of TiO$_2$ nanoparticles. *Chin. Sci. Bull.* **2011**, *56*, 1639–1657. [CrossRef]

27. Eskandarloo, H.; Badiei, A.; Behnajady, M.A.; Afshar, M. Enhanced photocatalytic removal of phenazopyridine by using silver-impregnated SiO$_2$–TiO$_2$ nanoparticles: Optimization of synthesis variables. *Res. Chem. Intermediat.* **2015**, *41*, 9929–9949. [CrossRef]

28. Liu, E.; Kang, L.; Wu, F.; Sun, T.; Hu, X.; Yang, Y.; Liu, H.; Fan, J. Photocatalytic reduction of CO$_2$ into methanol over Ag/TiO$_2$ nanocomposites enhanced by surface plasmon resonance. *Plasmonics* **2014**, *9*, 61–70. [CrossRef]

29. Kočí, K.; Zatloukalová, K.; Obalová, L.; Krejčíková, S.; Lacný, Z.; Čapek, L.; Hospodková, A.; Šolcová, O. Wavelength effect on photocatalytic reduction of CO$_2$ by Ag/TiO$_2$ catalyst. *Chin. J. Catal.* **2011**, *32*, 812–815. [CrossRef]

30. Kulkarni, R.M.; Malladi, R.S.; Hanagadakar, M.S.; Doddamani, M.R.; Bhat, U.K. Ag-TiO$_2$ nanoparticles for photocatalytic degradation of lomefloxacin. *Desalin. Water Treat.* **2016**, *57*, 1–8. [CrossRef]

31. Kočí, K.; Matějů, K.; Obalová, L.; Krejčíková, S.; Lacný, Z.; Plachá, D.; Čapek, L.; Hospodková, A.; Šolcová, O. Effect of silver doping on the TiO$_2$ for photocatalytic reduction of CO$_2$. *Appl. Catal. B-Environ.* **2010**, *96*, 239–244. [CrossRef]

32. Dilla, M.; Pougin, A.; Strunk, J. Evaluation of the plasmonic effect of Au and Ag on Ti-based photocatalysts in the reduction of CO$_2$ to CH$_4$. *J. Energy Chem.* **2017**, *26*, 277–283. [CrossRef]

33. Yu, B.; Zhou, Y.; Li, P.; Tu, W.; Li, P.; Tang, L.; Ye, J.; Zou, Z. Photocatalytic reduction of CO$_2$ over Ag/TiO$_2$ nanocomposites prepared with a simple and rapid silver mirror method. *Nanoscale* **2016**, *8*, 11870–11874. [CrossRef]

34. Pougin, A.; Dilla, M.; Strunk, J. Identification and exclusion of intermediates of photocatalytic CO$_2$ reduction on TiO$_2$ under conditions of highest purity. *Phys. Chem. Chem. Phys.* **2016**, *18*, 10809–10817. [CrossRef]

35. Dilla, M.; Schlögl, R.; Strunk, J. Photocatalytic CO$_2$ reduction under continuous flow high-purity conditions: Quantitative evaluation of CH$_4$ formation in the steady state. *ChemCatChem* **2017**, *9*, 696–704. [CrossRef]

36. Tampi, K.R.; Kiwi, J.; Grätzel, M. Methanation and photo-methanation of carbon dioxide at room temperature and atmospheric pressure. *Nature* **1987**, *327*, 506–508. [CrossRef]

37. Zhao, C.; Krall, A.; Zhao, H.; Zhang, Q.; Li, Y. Ultrasonic spray pyrolysis synthesis of Ag/TiO$_2$ nanocomposite photocatalysts for simultaneous H$_2$ production and CO$_2$ reduction. *Int. J. Hydrog. Energy* **2012**, *37*, 9967–9976. [CrossRef]

38. Thein, M.T.; Chim, J.E.; Punga, S.-Y.; Pung, Y.-F. Highly UV light driven WOx@ZnO nanocomposites synthesized by liquid impregnation method. *J. Ind. Eng. Chem.* **2017**, *46*, 119–129. [CrossRef]

39. Amadio, T.d.M.; Hotza, D.; Neto, J.B.R.; Blosi, M.; Costa, A.L.; Dondi, M. Bentonites functionalized by impregnation with TiO$_2$, Ag, Pd and Au nanoparticles. *Appl. Clay Sci.* **2017**, *146*, 1–6. [CrossRef]

40. Lee, K.-C.; Lin, S.-J.; Lin, C.-H.; Lin, C.-H.; Tsai, C.-S.; Lu, Y.-J. Size effect of Ag nanoparticles on surface plasmon resonance. *Surf. Coat. Tech.* **2008**, *202*, 5339–5342. [CrossRef]

41. Leong, K.H.; Gan, B.L.; Ibrahim, S.; Saravanan, P. Synthesis of surface plasmon resonance (SPR) triggered Ag/TiO$_2$ photocatalyst for degradation of endocrine disturbing compounds. *Appl. Surf. Sci.* **2014**, *319*, 128–135. [CrossRef]

42. Handoko, C.T.; Huda, A.; Bustan, M.D.; Yudono, B.; Gulo, F. Green synthesis of silver nanoparticle and its antibacterial activity. *Rasayan J. Chem.* **2017**, *10*, 1137–1144. [CrossRef]

43. Eom, H.; Jung, J.-Y.; Shin, Y.; Kim, S.; Choi, J.-H.; Lee, E.; Jeong, J.-H.; Park, I. Strong localized surface plasmon resonance effects of Ag/TiO$_2$ core–shell nanowire arrays in UV and visible light for photocatalytic activity. *Nanoscale* **2014**, *6*, 226–234. [CrossRef]

44. Handoko, C.T.; Huda, A.; Gulo, F. Synthesis pathway and powerful antimicrobial properties of silver nanoparticle: A critical review. *Asian J. Sci. Res.* **2019**, *12*, 1–17. [CrossRef]

45. Linic, S.; Christopher, P.; Ingram, D.B. Plasmonic-metal nanostructures for efficient conversion of solar to chemical energy. *Nat. Mater.* **2011**, *10*, 911–921. [CrossRef]

46. Boerigter, C.; Aslam, U.; Linic, S. Mechanism of charge transfer from plasmonic nanostructures to chemically attached materials. *ACS Nano* **2016**, *10*, 6108–6115. [CrossRef]

47. Shi, L.; Liang, L.; Ma, J.; Wang, F.; Sun, J. Enhanced photocatalytic activity over the Ag$_2$O–g-C$_3$N$_4$ composite under visible light. *Catal. Sci. Technol.* **2014**, *4*, 758–765. [CrossRef]

48. Wu, F.; Hu, X.; Fan, J.; Liu, E.; Sun, T.; Kang, L.; Hou, W.; Zhu, C.; Liu, H. Photocatalytic activity of Ag/TiO$_2$ nanotube arrays enhanced by surface plasmon resonance and application in hydrogen evolution by water splitting. *Plasmonics* **2012**, *8*, 501–508. [CrossRef]

49. Jahan, F.; Islam, M.H.; Smith, B.E. Band gap and refractive index determination of Mo-black coatings using several techniques. *Sol. Energy Mater. Sol. Cells* **1995**, *37*, 283–293. [CrossRef]

50. Uddin, M.T.; Nicolas, Y.; Olivier, C.; Jaegermann, W.; Rockstroh, N.; Junge, H.; Toupance, T. Band alignment investigations of heterostructure NiO/TiO$_2$ nanomaterials used as efficient heterojunction earth-abundant metal oxide photocatalysts for hydrogen production. *Phys. Chem. Chem. Phys.* **2017**, *19*, 19279–19288. [CrossRef] [PubMed]

51. Belver, C.; Hinojosa, M.; Bedia, J.; Tobajas, M.; Alvarez, M.A.; Rodríguez-González, V.; Rodriguez, J.J. Ag-coated heterostructures of ZnO-TiO$_2$/delaminated montmorillonite as solar photocatalysts. *Materials* **2017**, *10*, 960. [CrossRef] [PubMed]

52. Wang, S.; Qian, H.; Hu, Y.; Dai, W.; Zhong, Y.; Chen, J.; Hu, X. Facile one-pot synthesis of uniform TiO$_2$–Ag hybrid hollow spheres with enhanced photocatalytic activity. *Dalton Trans.* **2013**, *42*, 1122–1128. [CrossRef]

53. Duan, Y.; Zhang, M.; Wang, L.; Wang, F.; Yang, L.; Li, X.; Wang, C. Plasmonic Ag-TiO$_{2-x}$ nanocomposites for the photocatalytic removal of NO under visible light with high selectivity: The role of oxygen vacancies. *Appl. Catal. B-Environ.* **2017**, *204*, 67–77. [CrossRef]

54. Lei, T.; Xie, Y.; Wang, X.; Miao, S.; Xiong, J.; Yan, C. TiO$_2$ feather duster as effective polysulfides restrictor for enhanced electrochemical kinetics in lithium–sulfur batteries. *Small* **2017**, *13*, 1–9. [CrossRef] [PubMed]

55. Wang, Z.; Yang, C.; Lin, T.; Yin, H.; Chen, P.; Wan, D.; Xu, F.; Huang, F.; Lin, J.; Xie, X.; et al. Visible-light photocatalytic, solar thermal and photoelectrochemical properties of aluminium-reduced black titania. *Energy Environ. Sci.* **2017**, *6*, 3007–3014. [CrossRef]

56. Wang, Z.; Yang, C.; Lin, T.; Yin, H.; Chen, P.; Wan, D.; Xu, F.; Huang, F.; Lin, J.; Xie, X.; et al. H-doped black titania with very high solar absorption and excellent photocatalysis enhanced by localized surface plasmon resonance. *Adv. Funct. Mater.* **2013**, *23*, 5444–5450. [CrossRef]

57. Wang, F.; Zhang, S.; Li, C.; Liu, J.; He, S.; Zhao, Y.; Yan, H.; Wei, M.; Evans, D.G.; Duan, X. Catalytic behavior of supported Ru nanoparticles on the (101) and (001) facets of anatase TiO$_2$. *RSC Adv.* **2014**, *4*, 10834–10840. [CrossRef]

58. Chowdhury, I.H.; Ghosh, S.; Naskar, M.K. Aqueous-based synthesis of mesoporous TiO$_2$ and Ag–TiO$_2$ nanopowders for efficient photodegradation of methylene blue. *Ceram. Int.* **2016**, *42*, 2488–2496. [CrossRef]

59. Chen, L.; Hua, H.; Yang, Q.; Hu, C. Visible-light photocatalytic activity of Ag$_2$O coated Bi$_2$WO$_6$ hierarchical microspheres assembled by nanosheets. *Appl. Surf. Sci.* **2015**, *327*, 62–67. [CrossRef]

60. Rokade, A.A.; Patil, M.P.; Yoo, S.I.; Lee, W.K.; Park, S.S. Pure green chemical approach for synthesis of Ag$_2$O nanoparticles. *Green Chem. Lett. Rev.* **2016**, *9*, 216–222. [CrossRef]

61. Li, M.Y.; Mao, Y.Q.; Yang, S.K.; Dai, T.T.; Yang, H.; Feng, F.; Wu, T.; Chen, M.; Xu, G.Q.; Wu, J.H. Out-of-Substrate Ag−Ag$_2$O nanoplates: Surfactantless photochemical synthesis, structural evolution, and mechanistic study. *ACS Omega* **2016**, *1*, 696–705. [CrossRef]

62. Dilla, M.; Mateblowski, A.; Ristig, S.; Strunk, J. Photocatalytic CO$_2$ reduction under continuous flow high-purity conditions: Influence of light intensity and H$_2$O concentration. *ChemCatChem* **2017**, *9*, 4345–4352. [CrossRef]

63. Nasirian, M.; Mehrvar, M. Modification of TiO$_2$ to enhance photocatalytic degradation of organics in aqueous solutions. *J. Environ. Chem. Eng.* **2016**, *4*, 4072–4082. [CrossRef]

64. Sclafani, A.; Herrmann, J.-M. Influence of metallic silver and of platinum-silver bimetallic deposits on the photocatalytic activity of titania (anatase and rutile) in organic and aqueous media. *J. Photochem. Photobiol. A* **1998**, *113*, 181–188. [CrossRef]

65. Linsebigler, A.L.; Lu, G.; John, T.; Yates, J. Photocatalysis on TiO$_2$ surfaces: Principles, mechanisms, and selected results. *Chem. Rev.* **1995**, *95*, 735–758. [CrossRef]

66. Rtimi, S.; Baghriche, O.; Sanjines, R.; Pulgarin, C.; Bensimon, M.; Kiwi, J. TiON and TiON-Ag sputtered surfaces leading to bacterial inactivation under indoor actinic light. *J. Photochem. Photobiol. A* **2013**, *256*, 52–63. [CrossRef]

67. Busser, G.W.; Schuhmann, W.; Mei, B.; Pougin, A.; Willinger, M.-G.; Strunk, J.; Schlögl, R.; Gutkowski, R.; Muhler, M. Photodeposition of copper and chromia on gallium oxide: The role of co-catalysts in photocatalytic water splitting. *ChemSusChem* **2014**, *7*, 1030–1034. [CrossRef] [PubMed]

68. Phivilay, S.P.; Roberts, C.A.; Puretzky, A.A.; Domen, K.; Wachs, I.E. Fundamental bulk/surface structure−photoactivity relationships of supported $(Rh_2-yCryO_3)/GaN$ photocatalysts. *J. Phys. Chem. Lett.* **2013**, *4*, 3719–3724. [CrossRef]

69. Maeda, K.; Teramura, K.; Lu, D.; Saito, N.; Inoue, Y.; Domen, K. Roles of Rh/Cr_2O_3 (core/shell) nanoparticles photodeposited on visible-light-responsive $(Ga_{1-x}Zn_x)(N_{1-x}O_x)$ solid solutions in photocatalytic overall water splitting. *J. Phys. Chem. C* **2007**, *111*, 7554–7560. [CrossRef]

70. Domen, K.; Kudo, A.; Onishi, T. Mechanism of photocatalytic decomposition of water into H_2 and O_2 over $NiO-SrTiO_3$. *J. Catal.* **1986**, *102*, 92–98. [CrossRef]

71. Yoshida, M.; Takanabe, K.; Maeda, K.; Ishikawa, A.; Kubota, J.; Sakata, Y.; Ikezawa, Y.; Domen, K. Role and function of noble-metal/Cr-layer core/shell structure cocatalysts for photocatalytic overall water splitting studied by model electrodes. *J. Phys. Chem. C* **2009**, *113*, 10151–10157. [CrossRef]